NUMERICAL MODELING AND SIMULATION OF TURBULENT FLOW OF NEWTONIAN FLUIDS THROUGH POROUS MEDIA USING RANS AND LES APPROACH

Partha KUNDU[*], **Vimal KUMAR** and **Indra M. MISHRA**

Department of Chemical Engineering, Indian Institute of Technology Roorkee, Roorkee 247667, Uttarakhand, India
*Corresponding author, E-mail address: kundudch@iitr.ac.in

ABSTRACT

The numerical analysis of the mechanisms governing the flow in the porous region is of a priority interest for modeling porous media flows. The present study is a prerequisite for elaborating the efficient turbulence modeling techniques in porous media flows. The main objective of present study is to provide a detailed pore scale description of fluid flow and to analyze the formation of the coherent structures in the wake region close to the solid wall, subjected to the effects of the fine-scale turbulence. The computation was performed in a three dimensional representative elementary volume (*REV*) of porous media that are composed of a periodic array of circular cylinders. Two flow-modeling strategies were employed: steady RANS and the transient LES approach. In the RANS modeling framework both standard k–ε and low Re-k-ε turbulence models have been used. The porosity (ϕ) of the porous *REV* has been varied from 0.3 to 0.8 and Reynolds number based on cylinder diameter (Re_D) is varied from 100 to 40000. The effect of porosity and Re_D on pore scale velocity distribution, overall macroscopic pressure gradient and turbulence statics have been investigated. The detailed flow characteristics obtained from the RANS and LES calculations within the porous *REV* have been compared. The results of comprehensive computations over three dimensional *REV* is compared with analytical solutions of the Darcy–Forchheimer law. The good agreement between computational predictions and the empirical laws demonstrated the validity of the numerical method to simulate the macroscopic flow behavior in porous media.

NOMENCLATURE

$C_{1\varepsilon}$, $C_{2\varepsilon}$, $C_{3\varepsilon}$	model constants
D	cylinder diameter
f_1, f_2, f_μ	low Re-k-ε damping functions
H	center to center vertical distance between two circular cylinders (m)
Re_D	Reynolds number based on particle diameter
R_y	turbulent Reynolds number y ($y\sqrt{k}/v$)
R_T	turbulent Reynolds number ($k/v\varepsilon$)
k	turbulent kinetic energy (m²/s²)
$\langle k \rangle^f$	intrinsic volume average turbulence kinetic energy (m²/s²)
L	center to center horizontal distance between two circular cylinders (m)

$\langle p \rangle^f$	volume average pressure gradient (Pa)
Δt	time step
x,y,z	cartesian coordinates
$\overline{u}$	average fluid velocity (m/s)
u_D	Darcy velocity (m/s)
ϕ	medium porosity
μ	fluid viscosity (kg/m.s)
ρ	fluid density (kg/m³)
v	kinematic viscosity (m²/s)
ε	dissipation rate of k (m³/s²)
$\langle \varepsilon \rangle^f$	intrinsic volume average turbulence kinetic energy dissipation rate (m³/s²)
μ_t	turbulent (or eddy) viscosity (kg/m.s)
τ_{ij}	subgrid-scale stress
σ_{ij}	stress tensor
Π	filter function
$\Phi(x)$	filter variable

INTRODUCTION

Numerous geologic and engineering phenomena are governed by flow and transport processes through porous media. Turbulence phenomena in engineering flows and process industries will forever pose intellectually stimulating challenges. This flow behaviour is of great interest in various processes such as fluidized bed combustors, heat exchangers, enhanced oil reservoir recovery systems, combustion in an inert porous matrix, underground spreading of chemical wastes and chemical catalytic reactors (Kundu et al. 2012, 2014). Porous media also with their various morphologies are a challenging area of ongoing study.

In engineering and industrial flows at high Reynolds numbers, a complex interaction takes place between the instability due to the presence of the solid structure and the near-wall unsteady turbulence around the solid porous matrix. For accounting this interaction and predicting the unsteady hydrodynamics accurately, it is necessary to use reliable turbulence modeling approach. The large eddy simulation (LES) is appropriate and captures the turbulent flow physics in porous media at moderate to high Re. However, this approach is costly for design purposes at this stage (Shinde et al., 2014; Moussaed et al., 2014). LES was encouragingly used in turbulent flow in complex geometry (Palau-Salvador et al., 2008), submerged

vegetation (Stoesser et al., 2009), open channel flow, tube bundle (Rollet-Miet et al., 1999; Moussaed et al., 2014), wind flow around buildings of different configuration (Tutar and Oguz, 2002) etc. LES is able to provide an almost complete description of the instantaneous unsteady 3D turbulent flow field, resolving large-scale unsteadiness and asymmetries (large eddies) resulting from flow instabilities. It is always desired to visualize the actual flow physics inside the complex porous matrix. Turbulent flow covers a wide range of spatial and temporal scales. The numerical resolution of these turbulence scales requires high grid resolutions. The time-dependent and high resolution simulations based on large eddy simulation (LES) and Reynolds Averaged Navier–Stokes (RANS) models are able to provide the desired detailed porous media flow field predictions. Majority of research studies on modeling turbulent flows in porous media are based on the two equation k-ε model. Large eddy simulation of porous media flow is scarce. In order to fully understand the physics of the transitional/turbulent flows through the porous media and to capture the unsteady flow phenomena in the porous REV it is necessary to use eddy resolving techniques. However, there is increasing interest in applying LES to complex problems because of its greater accuracy over RANS, particularly for phenomena like turbulent porous media flow. LES approach is characterized by a division of the flow fields into large and small scales by a filtering procedure (Pope, 2005). LES can directly solve the equations that describe the evolution of a large range of turbulence scales. Only the smallest scales are modeled by LES using sub–grid–scale (SGS) models (Tajallipour, 2013). Study of turbulence flow modeling in porous media is limited in open literature. Moreover, large eddy simulation in porous media flow is very scare. Hence, a detailed numerical study of turbulent flow physics in porous media was presented.

The present work describes the prediction of flow in a three-dimensional porous media using both RANS and LES approaches. In the steady RANS modeling framework, two distinct turbulence models, namely standard k-ε and low Re-k-ε were used. The porous media studied, comprised an infinite array of circular cylinders and was characterized by medium porosity ($\phi = 0.3$–0.8). Numerical simulations were performed for flow over a wide range of Re_D ($Re_D = 100$-40000).

TURBULENCE MODELING

Reynolds Averaged Navier–Stokes (RANS) Turbulence Models

The continuity and RANS equations for turbulent flow of an incompressible viscous fluid are as follows:

Continuity equation:

$$\frac{\partial \rho}{\partial t} + \frac{\partial}{\partial x_i}\left(\rho \overline{u}_i\right) = 0 \tag{1}$$

RANS equation:

$$\frac{\partial}{\partial t}\left(\rho \overline{u}_i\right) + \frac{\partial}{\partial x_j}\left(\rho \overline{u}_i \overline{u}_j\right) = -\frac{\partial \overline{p}}{\partial x_i} + $$

$$\frac{\partial}{\partial x_j}\left[\mu\left(\frac{\partial \overline{u}_i}{\partial x_j} + \frac{\partial \overline{u}_j}{\partial x_i} - \frac{2}{3}\delta_{ij}\frac{\partial \overline{u}_l}{\partial x_l}\right) + \frac{\partial}{\partial x_j}\left(-\rho \overline{u_i' u_j'}\right)\right] \tag{2}$$

The Standard K-ε Turbulence Model
k equation:

$$\frac{\partial}{\partial t}\left(\rho k\right) + \frac{\partial}{\partial x_i}\left(\rho k \overline{u}_i\right) = \frac{\partial}{\partial x_j}\left[\left(\mu + \frac{\mu_t}{\sigma_k}\right)\frac{\partial k}{\partial x_j}\right] + G_k - \rho\varepsilon \tag{3}$$

ε equation :

$$\frac{\partial}{\partial t}\left(\rho\varepsilon\right) + \frac{\partial}{\partial x_i}\left(\rho \overline{u}_i \varepsilon\right) = \frac{\partial}{\partial x_j}\left[\left(\mu + \frac{\mu_t}{\sigma_\varepsilon}\right)\frac{\partial \varepsilon}{\partial x_j}\right] + $$

$$C_{1\varepsilon}\frac{\varepsilon}{k}G_k - C_{2\varepsilon}\rho\frac{\varepsilon^2}{k} \tag{4}$$

In equations (3) and (4), G_k represents the generation of turbulence kinetic energy due to the mean velocity gradients, and is defined as follows:

$$G_k = \mu_t S^2 \tag{5}$$

where S is the modulus of the mean rate-of-strain tensor and is defined as

$$S \equiv \sqrt{2\overline{S}_{ij}\overline{S}_{ij}} \tag{6}$$

$$\overline{S}_{ij} = \frac{1}{2}\left(\frac{\partial \overline{u}_i}{\partial x_j} + \frac{\partial \overline{u}_j}{\partial x_i}\right) \tag{7}$$

The turbulent (or eddy) viscosity μ_t is computed by combining k and ε as follows:

$$\mu_t = \rho C_\mu \frac{k^2}{\varepsilon} \tag{8}$$

The Low Re-K-ε Turbulence Model
k equation

$$\frac{\partial}{\partial x_i}\left(\rho \overline{u}_i k\right) = \frac{\partial}{\partial x_j}\left[\left(\mu + \frac{\mu_t}{\sigma_k}\right)\frac{\partial k}{\partial x_j}\right] + P_k - \rho\varepsilon \tag{9}$$

ε equation

$$\frac{\partial}{\partial x_i}\left(\rho \overline{u}_i \varepsilon\right) = \frac{\partial}{\partial x_j}\left[\left(\mu + \frac{\mu_t}{\sigma_\varepsilon}\right)\frac{\partial \varepsilon}{\partial x_j}\right] + $$

$$\left(C_{1\varepsilon}f_1 P_k - C_{2\varepsilon}f_2\rho\varepsilon\right)\frac{\varepsilon}{k} \tag{10}$$

$$P_k = -\rho \overline{u_i' u_j'}\frac{\partial \overline{u}_j}{\partial x_i}$$

Within the framework of eddy viscosity by adopting Boussinesq approximations, the Reynolds stresses are expressed as (Kundu et al. 2013):

$$-\rho \overline{u_i' u_j'} = \mu_t\left[\frac{\partial \overline{u}_j}{\partial x_i} + \left(\frac{\partial \overline{u}_j}{\partial x_i}\right)^T\right] - \frac{2}{3}\rho\delta_{ij}k \tag{11}$$

where, the turbulent viscosity is defined as

$$\mu_t = \rho C_\mu f_\mu \frac{k^2}{\varepsilon} \tag{12}$$

The damping functions account for the low-Reynolds number effects with enhanced wall effects and are given as (Yang, and Shih, 1993):

$$f_1 = f_2 = \frac{1}{1 + \dfrac{c_k}{\sqrt{R_T}}} \tag{13}$$

$$f_\mu = \left[1 - \exp \begin{pmatrix} -1.5 \times 10^{-4} \, R_y \\ -5.0 \times 10^{-7} \, R_y^3 \\ -1.0 \times 10^{-10} \, R_y^5 \end{pmatrix} \right]^{1/2} \quad (14)$$

The values of the model constants used for the numerical simulation are given as follows:

$$C_{1\varepsilon} = 1.44, C_{2\varepsilon} = 1.92, C_\mu = 0.09, C_{k=1},$$

$$\sigma_k = 1.0, \ \sigma_\varepsilon = 1.3$$

Large Eddy Simulation (LES)

LES is based upon the application of a spatial filtering operation (denoted by a bar) to the three dimensional (3D) unsteady Navier-Stokes (N-S) equations (Rollet-Miet et al., 1999). A filtered variable by the finite-volume discretization method is defined as:

$$\overline{\Phi}(x) = \frac{1}{V} \int_v \Phi(x') \, \Pi(x, x') \, dx', \quad x' \in v \quad (15)$$

where, V is the volume of a computational cell. The filter function, $\Pi(x, x')$ is

$$\Pi(x, x') \begin{Bmatrix} 1/V, & x' \in v \\ 0, & x' \, otherwise \end{Bmatrix} \quad (16)$$

Therefore, the filtered Navier-Stokes equation is:

$$\frac{\partial}{\partial t}(\rho \overline{u}_i) + \frac{\partial}{\partial x_j}(\rho \overline{u}_i \overline{u}_j) = \frac{\partial}{\partial x_j}\left(\mu \frac{\partial \sigma_{ij}}{\partial x_j} \right)$$

$$- \frac{\partial \overline{p}}{\partial x_i} - \frac{\partial \tau_{ij}}{\partial x_j} \quad (17)$$

where σ_{ij} is the stress tensor defined as

$$\sigma_{ij} \equiv \left[\mu \left(\frac{\partial \overline{u}_i}{\partial x_j} + \frac{\partial \overline{u}_j}{\partial x_i} \right) \right] - \frac{2}{3} \mu \frac{\partial \overline{u}_l}{\partial x_l} \delta_{ij} \quad (18)$$

and τ_{ij} is the sub–grid–scale stress is defined as

$$\tau_{ij} \equiv \rho \widetilde{u_i u_j} - \rho \overline{u}_i \overline{u}_j \quad (19)$$

Based on Boussinesq hypothesis (Hinze, 1975) and the Smagorinsky model (Smagorinsky, 1963), the sub–grid–scale turbulent stresses are expressed as

$$\tau_{ij} - \frac{1}{3} \tau_{kk} \delta_{ij} = -2\mu_t \overline{S}_{ij} \quad (20)$$

The filtered strain rate tensor for the resolved scale is defined by

$$\overline{S}_{ij} \equiv \frac{1}{2} \left(\frac{\partial \overline{u}_i}{\partial x_j} + \frac{\partial \overline{u}_j}{\partial x_i} \right) \quad (21)$$

The subgrid-scale eddy viscosity, can be estimated by the Smagorinsky model as follows:

$$\mu_t = \rho (C_s \Delta)^2 \left(2 \overline{S}_{ij} \overline{S}_{ij} \right)^{0.5} \quad (22)$$

where C_s is the Smagorinsky coefficient (Rodney et al., 2003), and Δ is the characteristic sub-grid length scale

Computational Model and Boundary Conditions

In the present study, the porous media was formed by a 3D infinite periodic array of circular cylinders. The fully developed macroscopic turbulent flow (incompressible

Newtonian fluid) was assumed to be uniform and parallel to the x–direction. Due to the symmetry (in y and z directions) and periodicity (in x direction) of the model, only one structural array cell (representative elementary volume, REV) with dimensions of 2H×1H×0.5H was chosen as the computational domain (Fig. 1). The Reynolds number based on cylinder diameter (D) i.e., $\mathrm{Re}_D = u_D \times D / \nu$ was varied between 100 and 40,000.

The porosity of the domain, $\phi = \left[1 - \frac{\pi}{4} \left(\frac{D}{H} \right)^2 \right]$, was varied between 0.3 and 0.8 (i.e. D/H = 0.94, 0.87, 0.80, 0.71 and 0.51).
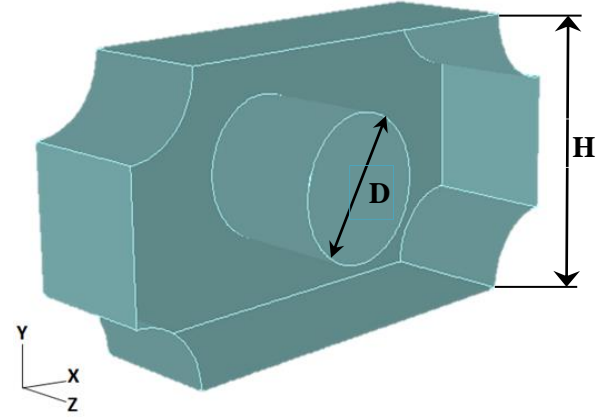
Figure 1: 3D porous representative elementary volume (REV).

The computational domain was constructed of a non-uniformly spaced staggered mesh system consisting of 1,083,700 nodes and 1,035,950 hexahedral cells. Preliminary calculations were made to compare the results against those obtained using coarse to fine mesh element having 528600, 1,083,700 and 1,362,322 nodes respectively for some selected cases. Very fine mesh resolution yielded no significant changes in the LES results, moreover it takes high computation time and cost, which proving that the originally used grid resolution was sufficient. The control volume finite difference method (CVFDM) was used for all simulation runs. The flow characteristics were obtained by solving the governing flow equations using ANSYS-FLUENT®14. The flow governing equations on the computational domain were discretized using second-order finite-volume schemes. For the time integration a central second-order implicit differencing scheme was employed. The pressure and velocity field coupling was done by the SIMPLE algorithm. The RANS flow calculations were performed with k-ε turbulence model using enhanced wall functions and with low Re-k-ε formulation. The unsteady LES calculations were performed using the Smagorinsky–Lilly SGS model (Lilly, 1966). The time-step used for all the simulation was (Δt =) 10^{-4} s. The convergence criterion is set to 10^{-4} for all simulations. The relaxation parameters for all variables $(\overline{u}, p, k, \varepsilon)$ were kept equal to 0.8.

Fully periodic boundary conditions were applied over *REV* for relevant variables. The periodic boundary conditions for the *REV* are as follows:

$$\left.\overline{u}(y)\right|_{x=0} = \left.\overline{u}(y)\right|_{x=2H} \qquad \left.\overline{v}(y)\right|_{x=0} = \left.\overline{v}(y)\right|_{x=2H}$$

$$\left.\overline{u}(x)\right|_{y=0} = \left.\overline{u}(x)\right|_{y=H} \qquad \left.\overline{v}(x)\right|_{y=0} = \left.\overline{v}(x)\right|_{y=H}$$
$$(23)$$

$$\left.k(y)\right|_{x=0} = \left.k(y)\right|_{x=2H} \qquad \left.\varepsilon(y)\right|_{x=0} = \left.\varepsilon(y)\right|_{x=2H}$$

$$\left.k(x)\right|_{y=0} = \left.k(x)\right|_{y=H} \qquad \left.\varepsilon(x)\right|_{y=0} = \left.\varepsilon(x)\right|_{y=H}$$
$$(24)$$

$$\left.\overline{p}(y)\right|_{x=0} = \left.\overline{p}(y)\right|_{x=2H} - \Delta p$$

$$\left.\overline{p}(x)\right|_{y=0} = \left.\overline{p}(x)\right|_{y=H}$$
$$(25)$$

Symmetry boundary conditions were considered at z = 0 and z = H/2:

$$\frac{\partial \overline{u}}{\partial z} = \frac{\partial \overline{v}}{\partial z} = \frac{\partial k}{\partial y} = \frac{\partial \varepsilon}{\partial y} = 0, \qquad \overline{w} = 0 \qquad (26)$$

Stationary wall (no-slip) boundary conditions are used for the arc-shaped corner boundary and center cylinder walls:

$$\overline{u} = \overline{v} = \overline{w} = 0 \qquad (27)$$

All fluid properties, including density and viscosity, are assumed constant for all simulations.

RESULTS

Microscopic Turbulent Flow Field

The simulated results of span wise velocity magnitude, pressure and turbulence kinetic energy contours for ϕ = 0.8, are shown in Figs. 2–3, in the computed REV. The fluid passes through the upper and lower surfaces of the cylinder having higher velocity magnitude, and flow separation takes place at the downstream of the front face of the cylinder. A larger wake region is formed at the downstream of the circular cylinder. The vortex or eddy formation is also observed at the corner circular surface in the upstream direction, where flow separation also takes place. The size of the vortex increases with an increase in Re_D and is dissipated upon travelling to downstream. At low Re_D the intensity of wake formation is low due to the fluid flowing smoothly over the entire circular cylinder. The turbulence increases downstream of the circular cylinder with an increase in Re_D, and the intensity of large wake region is generated in the form of eddies. At higher Reynolds number (Re_D = 40,000) complete flow separation takes place in the downstream section of the cylinder. The size of vortex at the downstream gets compressed gradually with a decrease in porosity, as the passage for fluid flow narrows down.

Fig. 2-3 shows that the maximum velocity magnitude is observed at the centre of the upstream section and upper and lower faces of the circular cylinder at a fixed value of ϕ. However, the flow gets separated from the back of the circular cylinder. A pair of stagnation points was formed at the centre of the upstream and the downstream face of the circular cylinder. A larger wake region is formed at the downstream of the circular cylinder which will contribute for larger pressure drop for the same mass flow rate through the porous media. In the remaining fields, it is observed that the pressure increases at the front of the

circular cylinder and decreases at the upper and lower faces.

As compared to LES the RANS simulations showed the excessively smooth turbulent structures within the REV, near the wall and around the cylindrical surface. The turbulent structures are overestimated. LES captures the turbulent flow features significantly well especially the near wall turbulent characteristics. The velocity and turbulent spectra are fluctuating in nature. From LES results, the spectra of instantaneous streamwise velocities show that a large region of low velocity is detached from the surface of cylinder into the wake and transported towards the stagnation point. The high magnitude velocity blobs occasionally entered into this region. These eddies are largely affected by the pore diameter and curvature of the wall. It seems that the turbulence kinetic energy is produced exclusively within the shear layers above the lateral surfaces of the cylinder, where the mean strain rate was quite high, which is different from that of the RANS model.
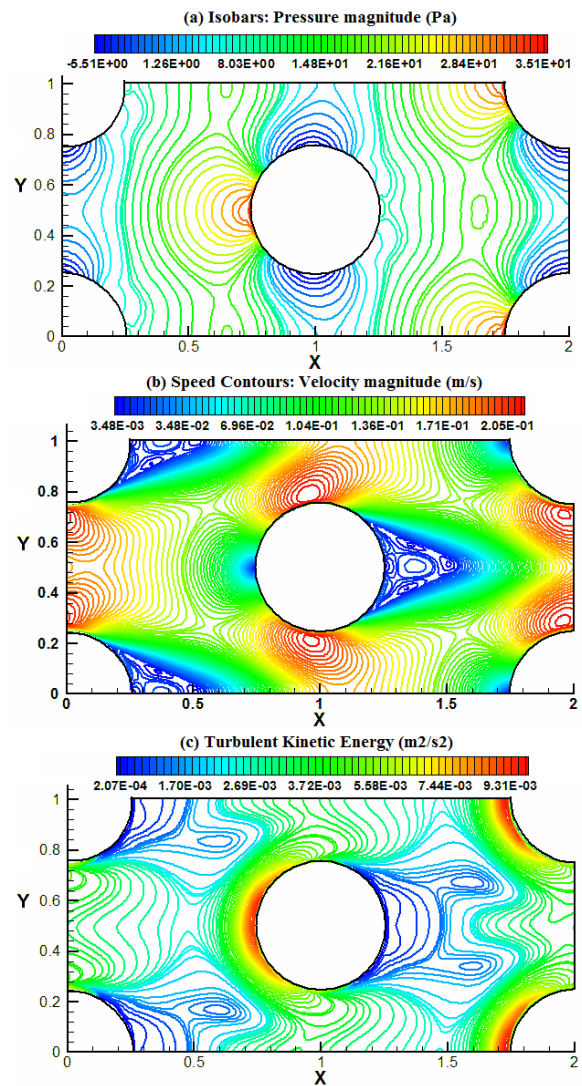
Figure 2: Simulated microscopic pressure, velocity and TKE contours of RANS simulation at ϕ = 0.8 and Re_D = 40000.

4

(a) Isobars: Pressure magnitude (Pa)

-6.47E+00 2.69E+00 8.33E+00 1.35E+01 1.90E+01 2.45E+01

(b) Speed Contours: Velocity magnitude (m/s)

7.13E-03 7.70E-02 1.34E-01 1.91E-01 2.18E-01 2.55E-01

(c) Turbulence Kinetic Energy (m2/s2)

9.26E-05 5.25E-04 1.02E-03 2.22E-03 3.33E-03 4.62E-03 5.83E-03
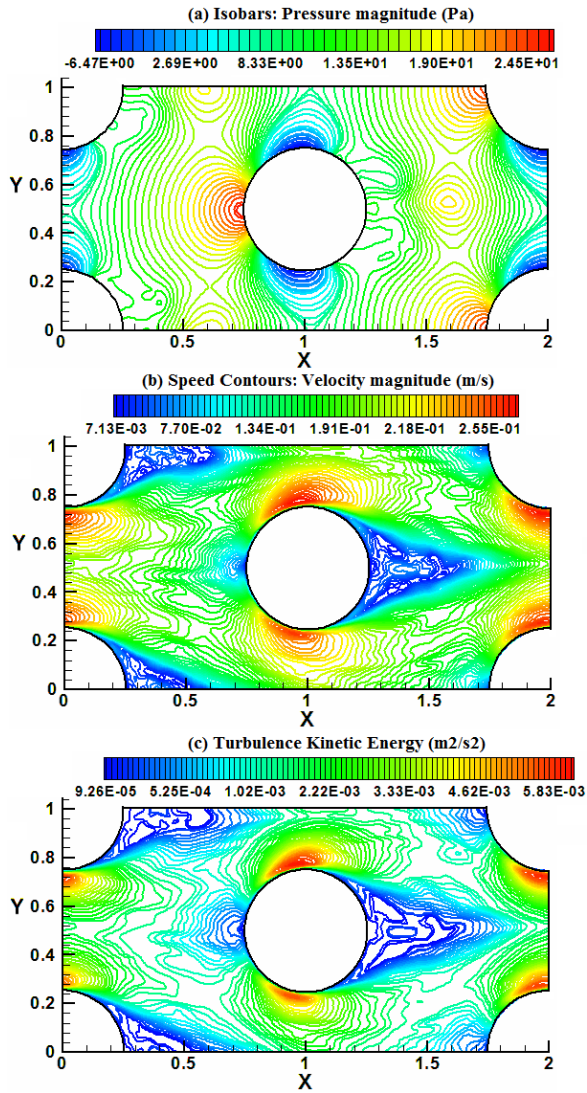
Figure 3: Simulated microscopic pressure, velocity and TKE contours of LES simulations at $\phi = 0.8$ and $Re_D = 40000$.

This is because of the fact that the conventional $k–\varepsilon$ model involves a k production term (P_k) (Eq. 9), which is coupled with the effective viscosity formulation. For a decelerating flow around the front stagnation point, extremely high production rate of k is observed, which leads to the over−estimation of the level of turbulence kinetic energy (Kuwahara et al. 1998; Kundu et al. 2014). This limitation can be overcome by LES approach which provides a reasonable turbulence kinetic energy distribution within the *REV*.

Computation of Macroscopic Turbulence Kinetic Energy and Dissipation Rate

LES and RANS simulated results of nomalized TKE are shown in Fig. 4 for $\phi = 0.8$. Similar trends were observed for other porosities. It is found that the normalized $\langle k \rangle^f$ increases with an increase in Re_D and a decrease in ϕ. It was observed that when $\phi < 0.6$, the increment is greater than unity even at lower Re_D. As the porosity decreases at a certain Re_D, the fluid flow passage gets reduced leading to an increase in the local fluid velocity

gradient. This, in turn, dictates the rate at which the mean flow mechanical energy gets transferred into turbulence kinetic energy. This causes the larger production rate of k within the REV. As a consequence, the normalized kinetic energy increases. It is also found that the turbulence gets intensified at a comparatively low Re_D, especially for low porosity.
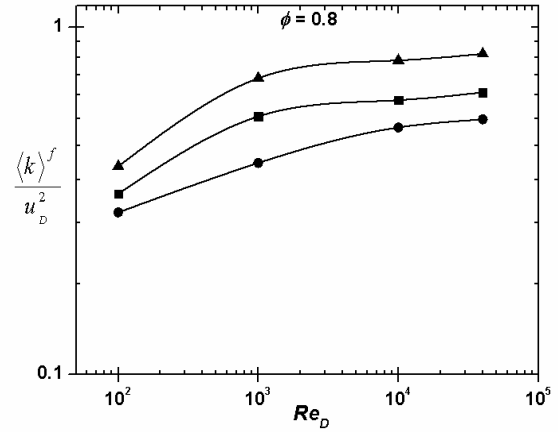
Figure 4: Normalized turbulence kinetic energy versus Re_D using various turbulence models. LES (−▲−); Low Re $k–\varepsilon$ (−■−); Std $k–\varepsilon$ (−●−).

It is observed that the LES and low Re-k-ε models show similar logarithmic patterns as compared to standard k-ε model, which shows a flat increment with Re_D. The low Re k-ε and LES predictions are reasonably well but standard k-ε model under predicts the normalized $\langle k \rangle^f$ for all values of ϕ. The normalized $\langle k \rangle^f$ for LES and low Re-k-ε model agreed significantly well in higher Re_D (>10³). However, no experimental results relevant to the porous *REV* are available in literature for comparison purpose.
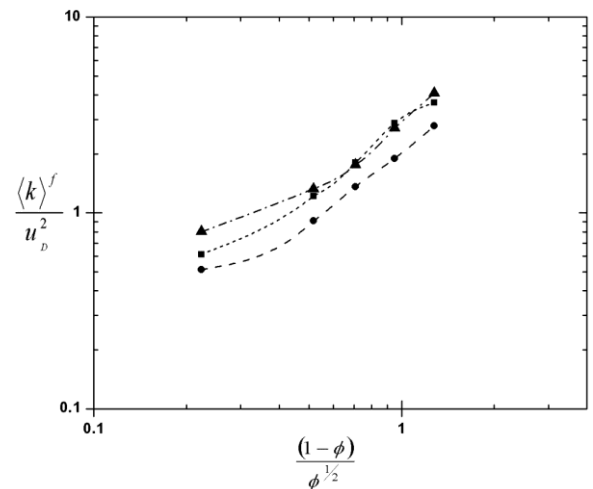
Figure 5(a): Normalized turbulent kinetic energy versus $(1−\phi)/\phi^{1/2}$ using different turbulence models. LES (−▲−); Low Re $k–\varepsilon$ (−■−); Std $k–\varepsilon$ (−●−).

For an infinite porous medium formed by staggered cylinders at high Re_D, the variation of turbulent kinetic energy with medium porosity is shown in Fig. 5(a). The

5

simulated normalized $\langle k \rangle^f$ predicted by LES and low Re k-ε model shows good agreement for $\phi < 0.8$. However, a deviation was observed at lower porosity ($\phi = 0.8$). The normalized dissipation rate $\langle \varepsilon \rangle^f$ for different porosities is shown in Fig. 5(b). At higher values of ϕ ($\phi = 0.6$ and 0.8) the predicted values of normalized $\langle \varepsilon \rangle^f$ by all the three different models followed similar trends. However, the results deviate at lower porosity ($\phi \leq 0.5$). Even at lower porosity the low Re-k-ε results are closer to the LES data.
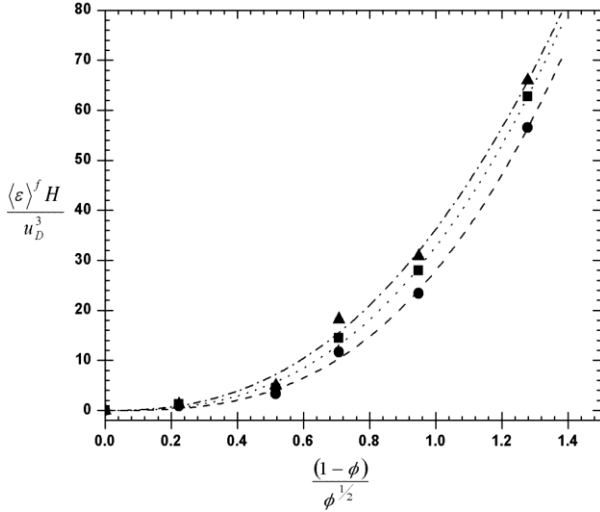
Figure 5(b): Normalized energy dissipation versus $(1-\phi)/\phi^{1/2}$ using different turbulence models. LES $(-\blacktriangle-)$; Low Re k-ε $(-\blacksquare-)$; Std k-ε $(-\bullet-)$.

Computation of Pressure Drop across the REV

The pressure distribution within the porous matrix is significantly influenced by the pore diameter. The pressure contours predicted by LES and RANS low Re k-ε model are shown in Figs. 2–3. It is observed that the pressure magnitude is high at the upstream face of the cylinder near to the stagnation point and at the downstream corner section of the *REV*. The macroscopic pressure gradient across the porous media as calculated using RANS low Re k-ε and LES methods are presented in a dimensionless manner.

The pressure drop across the porous REV can be estimated by the Ergun's equation. The Ergun's equation including the Forchheimer drag in the porous matrix of pore diameter of Dp, is given as (Kundu et al. 2013, 2014):

$$-\frac{d\langle p \rangle^f}{dx}\left[\frac{D_P}{\rho u_D^2}\right] = \frac{150(1-\phi)^2}{\phi}\left(\frac{\nu}{u_D D_P}\right) +$$
$$1.75\frac{1-\phi}{\phi^3} \qquad (28)$$

At higher Re_D, the viscous term disappears and the fluid inertial effect becomes significant. Therefore, at $Re_D > 3000$, Eq. (28) gets reduced to

$$-\frac{d\langle p \rangle^f}{dx}\left[\frac{D_P}{\rho u_D^2}\right] = 1.75\left(\frac{1-\phi}{\phi^3}\right) \qquad (29)$$

The variation of dimensionless macroscopic pressure gradient with medium ϕ is shown in Fig. 6. A linear relationship is anticipated with a coefficient of 1.75. The coefficient 2.2 is estimated by fitting the simulated data predicted by the turbulence model. The numerical results of the LES and RANS models agree well with the extended Forchheimer-Darcy's law within the porosity range, $0.8 \leq \phi \leq 0.5$, but at lower porosity, large deviation is observed.
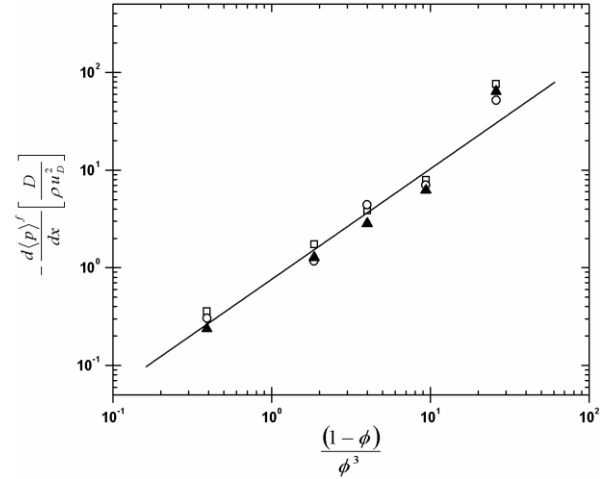
Figure 6: Dimensionless macroscopic pressure gradient versus $(1-\phi)/\phi^3$ using different turbulence models. LES $(-\blacktriangle-)$; Low Re k-ε $(-\square-)$; Std k-ε $(-\circ-)$.

CONCLUSION

In the present work comprehensive numerical simulations were performed for flow through porous media using steady RANS and transient LES methodology. The flow through porous media was formulated with three dimensional infinite periodic arrays of circular cylinders. Computations were performed over a wide range of porosity ($0.3 \leq \phi \leq 0.8$) and Reynolds number based on cylinder diameter ($100 \leq Re_D \leq 40000$). Extensive flow-fields, turbulence kinetic energy (TKE) and pressure distribution across the porous *REV* were presented to illustrate the complex pore flow phenomena. It was observed that the predicted flow-fields and TKE is strongly influenced by three-dimensional porous media with varying porosity and Re_D. Flow over the circular cylinder undergoes strong attenuation and enhancement of the turbulence and leads to flow separation and vortex formation. The pressure fields predicted by both RANS and LES were in good agreement; however, velocity and TKE fields were deviated. The anisotropic turbulent flow physics was not predicted by RANS simulation because of the unsteady nature of wakes formed within the REV. The unsteadiness was effectively captured using LES technique. The low Re k-ε results agreed well with the LES predictions. The macroscopic pressure gradient across the REV was computed as a function of porosity and Re_D. The numerical comparisons showed that the low Re k-ε results are the closest to the LES predictions.

REFERENCES

HINZE, J. O., (1975), "Turbulence", McGraw-Hill Publishing Co, New York.

KUNDU, P. KUMAR, V. and MISHRA, I. M., (2012), "Simulation of Turbulent Flows through Porous Media by k-ε Turbulent Model", *CHEMCON 2012,* India*, December 27-30.

KUNDU, P. KUMAR, V. and MISHRA, I. M., (2013), "Numerical Simulation of Fluid Flows through Porous Media using Low-Re Turbulence Model", *ACE 2013*, IIT Roorkee, India, February 22-24.

KUNDU, P. KUMAR, V. and MISHRA, I. M., (2014), "Numerical modeling of turbulent flow through isotropic porous media", *Int. J. Heat Mass Transfer*, **75**, 40–57.

KUWAHARA, F. KAMEYAMA, Y. YAMASHITA, S. and NAKAYAMA, A., (1998), "Numerical modelling of turbulent flow in porous media using a spatially periodic array", J. *Porous media,* **1**, 47-55.

LILLY, D. K., (1966), "On the application of the eddy viscosity concept in the inertial subrange of turbulence", *NCAR Manuscript*, **123**, 1-19.

MOUSSAED, C. SALVETTI, M. V. WORNOM, S. KOOBUS, B. and DERVIEUX, A., (2014), "Simulation of the flow past a circular cylinder in the supercritical regime by blending RANS and variational-multiscale LES models", *J. Fluids Structures*, **47**, 114–123.

PALAU-SALVADORA, G. STOESSERB, T. and RODIC, W., (2008), "LES of the flow around two cylinders in tandem", *J. Fluids Structures*, **24**, 1304–1312.

POPE, S. B., (2005). "Turbulent Flows", Cambridge University Press, Cambridge,

RODNEY, C. SCHMIDT, A. R. KERSTEIN, S. W. and VEBJORN, N., (2003), "Near-wall LES closure based on one-dimensional turbulence modeling", *J. Comput. Phys*, **186**, 317–355

ROLLET-MIET, P. LAURENCE, D. and FERZIGER, J., (1999), "LES and RANS of turbulent flow in tube bundles", *Int. J. Heat Fluid Flow*, **20**, 241-254.

SHINDE, V. MARCEL, T. HOARAU, Y. DELOZE, T. HARRAN, G. BAJ, F. CARDOLACCIA, J. MAGNAUD, J. P. LONGATTE, E. and BRAZA, M., (2014), "Numerical simulation of the fluid–structure interaction in a tube array under crossflow at moderate and high Reynolds number", *J. Fluids Structures*, **47**, 99–113.

SMAGORINSKY, J., (1963), "General Circulation Experiments with the Primitive Equations. I. The Basic Experiment"*, Month. Wea. Rev*, **91**, 99-164.

STOESSER, T. SALVADOR, G. P. RODI, W. and DIPLAS, P., (2009), "Large Eddy Simulation of Turbulent Flow Through Submerged Vegetation", *Transp. Porous Media*, **78**, 347–365.

TAJALLIPOUR, N. KUMAR, V. and PARASCHIVOIU, M., (2013), "Large-eddy simulation of a compressible free jet flow on unstructured elements", *Int. J. Numer. Meth. Heat & Fluid Flow,* **23**, 336-354.

YANG, Z. and SHIH, T. H., (1993), "New time scale based k-ε model for near-wall turbulence", *AIAA J.* **31**, 1191 – 1198.